# Numerical study of viscous effects during CPTu

*Laurin* Hauser[1#], *Diego* Durán[12], *Lluís* Monforte[1], *Marcos* Arroyo[2], and *Antonio* Gens[2]

[1]*Centre Internacional de Mètodes Numèrics en Enginyeria (CIMNE)*
*Campus Nord UPC, Carrer Jordi Girona, 1-3, Edifici C1, 08034 Barcelona, Spain*

[2]*Universitat Politècnica de Catalunya (UPC)*
*Campus Nord UPC, Carrer Jordi Girona, 1-3, Edifici D2, 08034 Barcelona, Spain*

[#]*Corresponding author: laurin.hauser@upc.edu*

## ABSTRACT

Variable penetration rates during CPTu may impact cone readings through partial consolidation during penetration but also through viscous soil skeleton behaviour. The latter phenomenon is characteristic of dynamic penetrometers during fast penetration in fine-grained materials where tip resistance increases when the penetration rate increases. In this work, the effect of viscosity on piezocone penetration is investigated based on the numerical simulation of CPTu and triaxial tests using the application G-PFEM and a viscoplastic version of the Clay and Sand Model (CASM). The study highlights that the CPTu results are sensitive to the material parameters controlling viscosity, thus requiring careful calibration in order to obtain realistic CPTu simulations.

**Keywords:** CPTu, rate effects, viscoplasticity, CASM-Visco.

## 1. Introduction

The penetration rate of the penetrometer is known to influence the tip resistance and pore pressure measured during piezocone penetration testing (CPTu). Two different phenomena underlie those changes: partial consolidation and viscous behaviour (Lehane et al. 2009).

The effect of drainage on cone measurements has been extensively studied (De Jong & Randolph, 2012; Martinez et al. 2016; Bihs et al. 2021) as it has a major impact on the interpretation of standard CPTu measurements ($v$ = 2 cm/s) in silts and other intermediate soils. Increased drainage results in larger tip resistance and lower pore pressure; this is observed during testing at variable penetration rates in the same site. The effect of partial drainage on cone penetration has also been observed in CPTu simulation by changing penetration rate, permeability or both (e.g. Monforte et al. 2018).

Viscous effects on CPTu measurements are most significant for free-fall or dynamic CPTu tests that are frequently employed in offshore site investigation. These effects have been mainly studied from an empirical perspective, using relatively simple interpretation models (Steiner et al. 2014; Collico et al. 2022).

The present work aims to investigate the effect of variable penetration rates on CPTu results for soils with a significant viscous response by means of numerical simulations with the G-PFEM platform (Carbonell et al. 2022). Fully-coupled hydromechanical analyses are performed using a viscoplastic constitutive model. After reviewing the constitutive model and examining the influence of viscosity through element testing, the effect of a variable penetration rate is investigated.

## 2. Numerical model

### 2.1. G-PFEM

The application G-PFEM is an implementation of the Particle Finite Element Method (Oñate et al. 2004) within the Kratos Multiphysics framework to address insertion problems in geotechnical engineering considering large deformations, frictional contact, and non-linear constitutive models Monforte et al. (2018). G-PFEM has already been successfully applied to simulate cone penetration in complex soils and under various drainage conditions (Monforte et al. 2021; Hauser and Schweiger 2021; Boschi et al. 2024).

### 2.2. Viscoplastic CASM (CASM-Visco)

The Clay and Sand Model (CASM; Yu, 1998) is an isotropic, state parameter-based, elasto-plastic model formulated within the critical state (CS) framework. The shape of the yield surface is controlled by two constitutive parameters: the spacing ratio $r$ and the shape parameter $n$, which makes the model adaptable for a wide range of soils. The yield surface is defined as:

$$f = \left(\frac{q}{p' M_\theta}\right)^n + \frac{1}{\ln r} \ln \frac{p'}{p'_0} \tag{1}$$

where $p'$, $q$, $\Theta$ are the effective mean stress, the deviatoric stress invariant, and the Lode angle, respectively. $M_\Theta$ is the stress ratio at CS depending on $\Theta$ (the Mohr-Coulomb failure criterion is adopted in the deviatoric plane), and $p'_0$ is the preconsolidation pressure. Well-established models, such as the Original or the Modified Cam clay model, may be recovered for specific choices of $r$ and $n$.

The G-PFEM implementation of the model features a non-associated flow rule where the plastic potential (Mánica et al. 2022) is:

$$g = \left(\frac{q}{p' M_\theta}\right)^m + m - \frac{\zeta(m-1)}{p'} - 1 \tag{2}$$

Where $m$ is a constitutive parameter. $\zeta$ is a scalar such that the current stress state lies on the plastic potential surface.

CASM-Visco is a viscoplastic extension of CASM based on the overstress concept by Perzyna (1966), first presented in Arroyo & Gens (2021) and Mánica et al. (2021). The viscoplastic rate constitutive equations at small strains are summarised as follows using Voigt notation:

$$\begin{cases} \dot{\boldsymbol{\epsilon}} = \dot{\boldsymbol{\epsilon}}^e + \dot{\boldsymbol{\epsilon}}^{vp} \\ \dot{\boldsymbol{\sigma}}' = \mathbf{D}(\boldsymbol{\sigma}') \cdot \dot{\boldsymbol{\epsilon}}^e \\ \dot{\boldsymbol{\epsilon}}^{vp} = \dot{\gamma}\, \boldsymbol{m} \\ \dot{\boldsymbol{\chi}} = \dot{\gamma}\, \mathbf{h}(\boldsymbol{\sigma}', \boldsymbol{\chi}) \\ \dot{\gamma} = \frac{\langle \Phi(f) \rangle^N}{\eta} \end{cases} \tag{3}$$

The total strain tensor $\boldsymbol{\epsilon}$ is decomposed additively into an elastic ($\boldsymbol{\epsilon}^e$) and viscoplastic ($\boldsymbol{\epsilon}^{vp}$) part. The effective stress tensor $\boldsymbol{\sigma}'$ is related to the elastic strain tensor through the elastic stiffness matrix $\mathbf{D}(\boldsymbol{\sigma}')$ which features a pressure-dependent bulk and shear modulus:

$$K = \frac{p'}{\kappa^*} \qquad G = \frac{3(1-2\nu)}{2(1+\nu)} K \tag{4}$$

with $\kappa^*$ and $\nu$ being the modified swelling slope and the Poisson's ratio, respectively. The viscoplastic strains $\boldsymbol{\epsilon}^{vp}$ evolve according to the non-associated flow rule with $\dot{\gamma}$ being the incremental plastic multiplier and $\boldsymbol{m} = (\partial g/\partial \boldsymbol{\sigma}')/\|\partial g/\partial \boldsymbol{\sigma}'\|$ being the normalised plastic flow direction. The vector of hardening variables ($\boldsymbol{\chi}$) reduces to a scalar quantity for the *CASM*. Thus, the evolution equation for $p'_0$ yields:

$$\dot{\boldsymbol{\chi}} = \dot{p}'_0 = \dot{\gamma} \frac{p'_0}{\lambda^* - \kappa^*} \left(\frac{\partial g}{\partial p'}\right) \Big/ \left\| \frac{\partial g}{\partial \boldsymbol{\sigma}'} \right\| \tag{5}$$

with the modified isotropic compression slope $\lambda^*$.

The incremental plastic multiplier depends on the overstress function

$$\Phi(f) = \left(\frac{f(\boldsymbol{\sigma}', \boldsymbol{\chi})}{f_0}\right) \tag{6}$$

with $f_0$ being a reference value for $f$ and $\eta$ and $N$ are constitutive parameters. Viscoplastic flow is assumed to occur when the yield condition is violated:

$$\langle \Phi(f) \rangle = \begin{cases} \Phi(f) & \text{if} \quad \Phi(f) \geq 0 \\ 0 & \text{if} \quad \Phi(f) < 0 \end{cases} \tag{7}$$

Note that inviscid behaviour may be obtained for $\eta \to 0$. Details on the extension of the model to tackle finite strains and the implementation in *G-PFEM* are omitted here (Hauser et al. 2024).

## 3. Results and discussion

The following numerical study is inspired by the work of Robinson (2019) on rate effect behaviour of clays. Thus, the adopted CASM constitutive parameters, summarised in Table 1, are representative of Kaolin clay, as used by Robinson (2019) to conduct triaxial tests at variable strain rates. The basic CASM parameters were calibrated assuming inviscid behaviour while the viscous constitutive parameters $\eta$ and $N$ were defined based on the literature: Arroyo and Gens (2021) analyzed the Brumadinho dam failure using CASM-Visco, indicating that $\eta$ = 1.0E-9 m² day kN$^{-1}$ and $N$ = 5 are suitable for the investigated tailings materials based on variable strain rate triaxial tests. For plastic clays, though, usually more pronounced viscous effects are observed. Pinedo et al. (2022) showed that $\eta$ = 6.6E-6 m² day kN$^{-1}$ and $N$ = 3 to 4 results in an increase in undrained shear strength of around 10% per log cycle of strain rate, which is typically observed for plastic clays. In the present work, $\eta$ = 1.2E-7 m² day kN$^{-1}$ and $N$ = 5 are used.

To characterize the effect of viscous behaviour for the considered soil, the results of anisotropically consolidated ($K_0$ = 0.62) undrained triaxial element tests adopting different strain rates are shown in Fig. 1 and Fig 2: The undrained shear strength increases by up to 7 % per log cycle of strain rate (see Fig. 1). In contrast, the excess pore pressure shows the opposite trend and reduces with increasing strain rate (see Fig. 2).

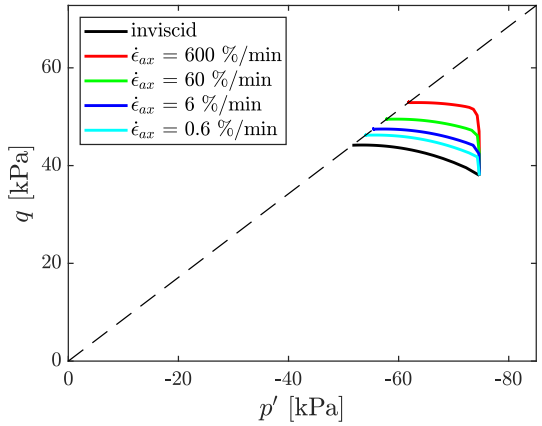


**Figure 1.** Stress path of undrained triaxial tests for inviscid and viscoplastic soil, adopting different strain rates.

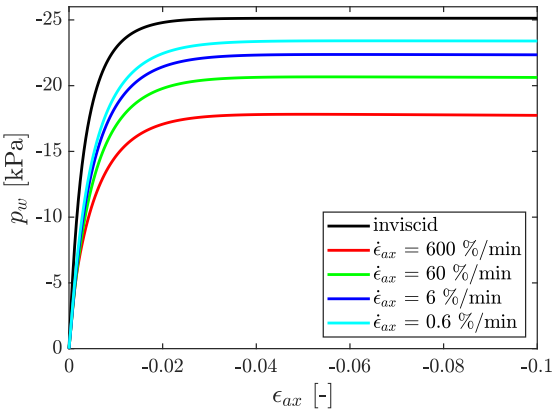


**Figure 2.** Evolution of pore water pressure during undrained triaxial tests for inviscid and viscoplastic behaviour, adopting different strain rates.

**Table 1.** CASM parameters representative of Kaolin.

| **φ'** [°] | **λ* [-]** | **κ* [-]** | **ν** [-] | **r** [-] | **n** [-] | **m** [-] |
|---|---|---|---|---|---|---|
| 22 | 0.072 | 0.009 | 0.3 | 2.125 | 1.6 | 3 |

### 3.1. Triaxial testing

In the next step, triaxial compression tests adopting different strain rates were simulated as a boundary value problem. The strain rate range was based on Robinson (2019), and the tests were modelled as an axisymmetric problem (see Fig. 3). The height and radius of the specimen are 20 cm and 5 cm, respectively. The displacements are fixed in the normal direction along the left lateral boundary (i.e. the symmetry axis) and in both directions along the bottom boundary. On the top boundary, a vertical velocity $\dot{u}_v$ is prescribed, reaching a final vertical displacement of 4 cm. Free drainage is allowed along the right lateral boundary, analogously to the experimental setup of Robinson (2019). Furthermore, a constant initial stress field with $\sigma'_v$ = 100 kPa, $\sigma'_h$ = 62 kPa, and $u_0$ = 0 kPa is applied while $\sigma_h$ = 62 kPa is held constant during the test. A soil permeability $k$ = 1.0E-9 m/s and an OCR = 1.05 were assumed.

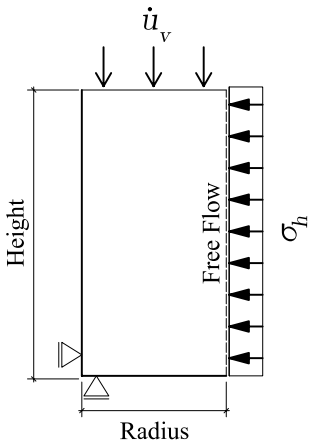


**Figure 3.** Axisymmetric model of triaxial testing.

The vertical reaction forces at the top of the domain were used to calculate the averaged total vertical stress $\sigma_v$ and the resulting deviatoric stress $q = \sigma_v - \sigma_h$. Fig. 4 shows the normalized peak deviatoric stress $q/q_{ref}$ for different strain rates considering inviscid (CASM) and viscous (CASM-Visco) material behaviour. Note that $q_{ref}$ corresponds to the peak deviatoric stress obtained for inviscid material under undrained conditions, i.e., strain rates larger than 1.0E-1 %/min.

As expected, the rate effect due to consolidation is observable for the inviscid material where the respective maximum and minimum values for $q/q_{ref}$ are reached for drained ($\dot{\epsilon}_{ax}$ < 1.0E-5 %/min) and undrained ($\dot{\epsilon}_{ax}$ > 1.0E-1 %/min) conditions. When viscous behaviour is considered, its effect becomes evident for $\dot{\epsilon}_{ax}$ between 1.0E-3 and 1.0E-2 %/min, where slightly higher deviatoric stresses are obtained compared to the inviscid case. The minimum $q$ is observed for strain rates between 1.0E-2 and 1.0E-1 %/min. For larger strain rates, viscous behaviour becomes dominant, resulting in increased $q/q_{ref}$. The observed trend agrees with the laboratory results reported by Robinson (2019) for isotropically consolidated specimens where the undrained shear strength increases by 11 to 14% per log cycle increase in strain rate. The numerical results indicate a slightly lower strength increase of up to 9% per log cycle increase in strain rate. This is expected, as (i) anisotropically consolidated samples were considered in the present study, and (ii) the viscous parameters that control the response were not calibrated for Kaolin but were just chosen. Work is ongoing on a simple and effective calibration procedure for these viscous parameters.

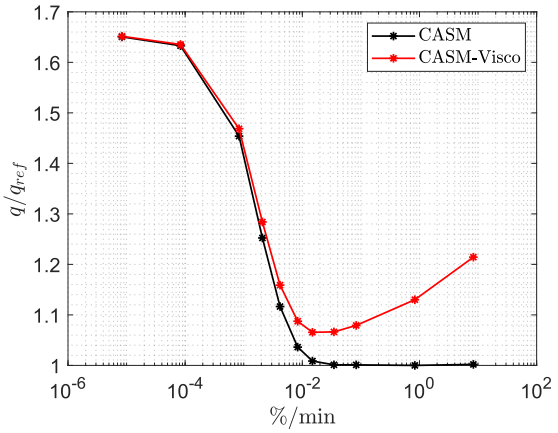


**Figure 4.** Normalized deviatoric stress from triaxial compression tests using different strain rates.

### 3.2. CPTu penetration

CPTu simulations using different penetration velocities were carried out for the same material. The axisymmetric model is illustrated in Fig. 5 and has a height $h$ of 1 m and a width $b$ of 0.5 m. Displacements at the bottom boundary are fixed, while vertical displacements are free in the lateral boundaries. The model boundaries are free-draining except for the vertical symmetry axis. Assuming weightless soil, the same constant initial stress field as used for the triaxial testing is prescribed ($\sigma'_{v0}$ = 100 kPa, $\sigma'_{h0}$ = 62 kPa). In addition, the total vertical overburden stress $\sigma_{v0}$ is specified along the top boundary. The rigid cone is initially inserted in the soil at a depth $h_1$ of 0.2 m. Penetration is simulated by prescribing a downward displacement at a given velocity $v$. Velocities of 0.2 and 20 cm/s were used in addition to the standard penetration velocity of 2 cm/s. For simplicity, no friction between the penetrometer and the soil is considered. However, this is no limitation of the model. Monforte et al. (2021) showed that interface friction leads to an increase in $q_t$ and a reduction in $u_2$.

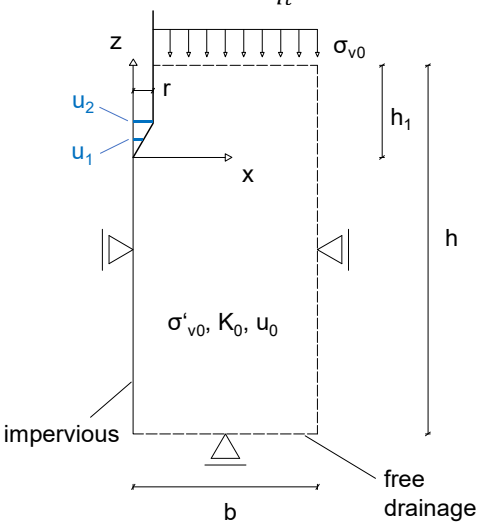


**Figure 5.** Axisymmetric model for CPTu penetration.

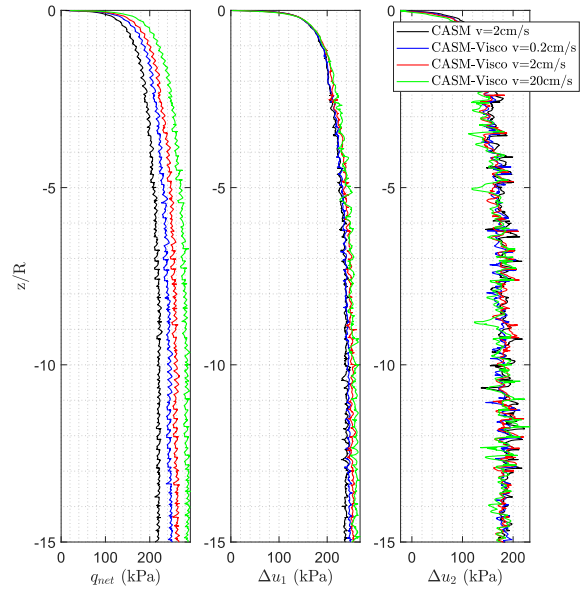


**Figure 6.** Normalized depth profiles of simulated net cone resistance ($q_{net}$) and excess pore pressures ($\Delta u_1$, $\Delta u_2$).

The simulated net cone resistance $q_{net} = q_t - \sigma_{v0}$ and the excess pore pressures $\Delta u_1$ and $\Delta u_2$, measured at the cone centre and shoulder, respectively, are plotted over the normalized cone tip depth $z/R$ in Fig. 6. Note that for inviscid behaviour, only the standard velocity of 2 cm/s is plotted since all velocities result in practically undrained conditions and, thus, almost identical CPTu measurements. After an initial transient phase of around 8 to 10 radii of penetration, steady-state values are reached. In the following, the average between 10 and 15 radii of penetration is taken as the representative value for $q_{net}$, $\Delta u_1$, and $\Delta u_2$, respectively. Fig. 7 shows the net cone resistance normalized by $q_{net,ref}$, corresponding to inviscid behaviour and $v = 2$ cm/s, for different penetration velocities. As noted, the tip resistance for inviscid soil is insensitive to a change in $v$, indicating undrained behaviour for the considered penetration velocities.

When viscosity is introduced, higher tip resistances are obtained compared to the inviscid undrained reference case, up to almost 20 % for the standard velocity of 2 cm/s. The increase in tip resistance with $v$ falls within the range proposed by Lunne et al. (1997) based on field studies, suggesting that $q_c$ increases by 7.5

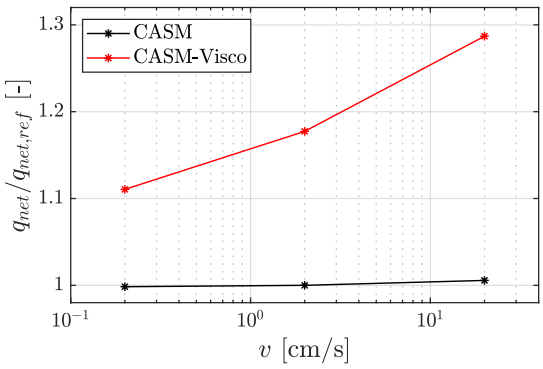


**Figure 7.** Normalized net cone resistance $q_{net}/q_{net,ref}$ over penetration velocity.

to 20 % per log cycle increase in penetration velocity above the standard penetration velocity of 2 cm/s for typical clays. Furthermore, Bemben and Myers (1974) and Roy et al. (1982) reported for varved and silty clays that the minimum tip resistance is reached for $v = 0.2$ cm/s. The presented results confirm that $v < 2$ cm/s leads to a lower $q_{net}$ in undrained conditions.

The evolution of normalized excess pore pressures $\Delta u_1$ and $\Delta u_2$ is shown in Fig. 8 and Fig. 9, respectively. Again, the excess pore pressures obtained for the inviscid behaviour and $v = 2$ cm/s are used as reference. For the inviscid material, conditions remain undrained for all velocities, with negligible variation of pore pressure between the analyses (< 2.5 % for $\Delta u_2$). In general, the pore pressures appear almost insensitive to rate effects also for viscous material, as the magnitude of increase in $\Delta u_1$ with $v$ remains relatively small. It is noteworthy that the $u_1$ pressures are larger compared to the inviscid case, while the $u_2$ pressures are smaller. Furthermore, $\Delta u_1$ increases with $v$ while $\Delta u_2$ appears to remain somewhat constant, indicating a decrease with higher $v$. To confirm this trend, however, further analyses are required, as the variations are small and numerical noise is significant, particularly for the $u_2$ record.

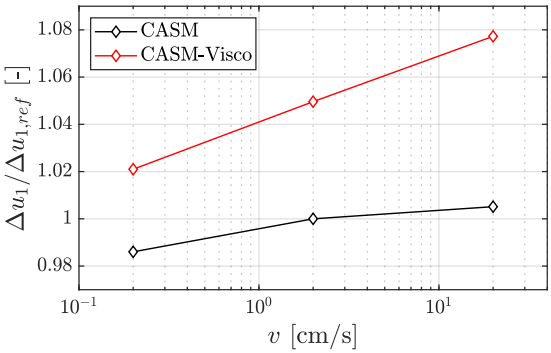


**Figure 8.** Normalized excess pore pressure $\Delta u_1/\Delta u_{1,ref}$ over penetration velocity.

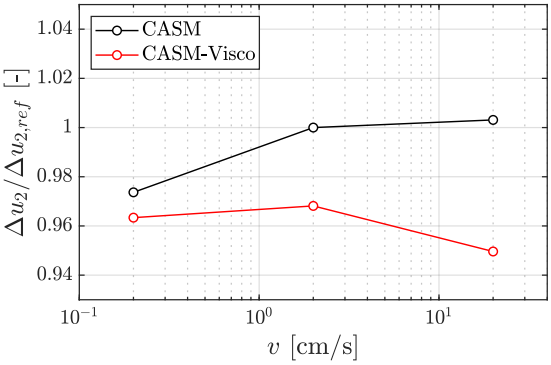


**Figure 9.** Normalized excess pore pressure $\Delta u_2/\Delta u_{2,ref}$ over penetration velocity

## 4. Conclusions

This paper explores viscous effects on CPTu measurements through numerical analyses using a viscoplastic constitutive model (CASM-Visco). The presented results, which should be understood as the outcome of a preliminary study, show that viscosity leads to an increase in tip resistance of around 20% compared to the corresponding inviscid case for undrained

penetration in clays with the standard penetration velocity of 2 cm/s. Although the observed increase in tip resistance per log cycle increase in penetration velocity agrees with field observations, more work is required to calibrate the viscous constitutive parameters $\eta$ and $N$ and further understand their influence on the CPTu results. The tip resistance obtained from CPTu testing and the peak deviatoric stress resulting from triaxial testing show very similar behaviour when subjected to a change in penetration velocity or loading rate, respectively. Further research is needed to explore ways to link the two quantities.

## Acknowledgements

The authors gratefully acknowledge the financial support of Ministerio de Ciencia, Innovación y Universidades of Spain (MCIN/AEI/10.13039/501100011033) through the research grant PID2020-119598RB-I00.

## References

Arroyo, M., Gens, A., "Computational analyses of Dam I failure at the Corrego de Feijao mine in Brumadinho", CIMNE, Barcelona, Spain, Final report, 2021.

Bemben, S.M., Myers, H.J., "The influence of rate of penetration on static cone resistance in Connecticut river valley varved clay", Proceedings of the European symposium on penetration testing, Stockholm, Sweden, pp. 33-34, 1974.

Bihs, A., Long, M., Nordal, S., Paniagua, P., "Consolidation parameters in silts from varied rate CPTU tests", AIMS Geosciences, 7(4), pp. 637-68, 2021. https://doi.org/10.3934/geosci.2021039

Boschi, K., Arroyo, M., Monforte, L., Carbonell, J.M., Gens, A., "Coupled hydromechanical modelling of cone penetration in layered liquefiable soils", Géotechnique, 2024. https://doi.org/10.1680/jgeot.23.00164

Carbonell, J.M., Monforte, L., Ciantia, M.O., Arroyo, M., Gens, A., "Geotechnical particle finite element method for modeling of soil-structure interaction under large deformation conditions", Journal of Rock Mechanics and Geotechnical Engineering 14, issue 3, pp. 967-983, 2022. https://doi.org/10.1016/j.jrmge.2021.12.006

Collico, S., Arroyo, M., Kopf, A., Devincenzi, M., "A probabilistic Bayesian methodology for the strain-rate correction of dynamic CPTu data", Canadian Geotechnical Journal, 60(5), pp. 669-686, 2022. https://doi.org/10.1139/cgj-2022-0311

DeJong, J. T., Randolph, M., "Influence of partial consolidation during cone penetration on estimated soil behavior type and pore pressure dissipation measurements", Journal of Geotechnical and Geoenvironmental Engineering, 138(7), pp. 777-788, 2012. https://doi.org/10.1061/(ASCE)GT.1943-5606.0000646

Hauser, L., Schweiger, H.F., "Numerical study on undrained cone penetration in structured soil using G-PFEM", Computers and Geotechnics 133, 104061, 2021. https://doi.org/10.1016/j.compgeo.2016.08.013

Hauser, L., Monforte, L., Carbonell, J.M., Arroyo, M., Gens, A., "A nonlocal elasto-viscoplastic model for structured soils at large strains (Cem-CASMv): formulation and implementation", in preparation.

Lehane, B.M., O'Loughlin, C.D., Gaudin, C., "Rate effects on penetrometer resistance in kaolin", Géotechnique 59, no. 1, pp. 41–52, 2009. https://doi.org/10.1680/geot.2007.00072

Lunne, T., Robertson, P.K., Powell, J.J., "Cone penetration testing in geotechnical practice", London, Blackie Academic & Professiona, 1997.

Mánica, M., Arroyo, M., Gens, A., "Effects of tailings viscosity on liquefaction triggering analyses", Proceedings of the Tailings and Mine Waste Conference 2021 (TMW 2021), Banff, Alberta, Canada, pp. 372-380, 2021.

Mánica, M., Arroyo, M., Gens, A., Monforte, L., "Application of a critical state model to the Merriespruit tailings dam failure", Proceedings of the Institution of Civil Engineers - Geotechnical Engineering 175, issue 2, pp. 151–165, 2022. https://doi.org/10.1680/jgeen.21.00001

Martinez, M.G., Tonni, L., Gottardi, G. "On the interpretation of piezocone tests in natural silt and sand mixtures", Proceedings of the 4th International Symposium on Cone Penetration Testing (CPT'18), Delft, Netherlands, pp. 63-68, 2018.

Monforte, L., Arroyo, M., Carbonell, J.M., Gens, A., "Coupled effective stress analysis of insertion problems in geotechnics with the Particle Finite Element Method", Computers and Geotechnics 101, pp. 114–129, 2018. https://doi.org/10.1016/j.compgeo.2018.04.002

Monforte, L., Gens, A., Arroyo, M., Mánica, M., Carbonell, J.M., "Analysis of cone penetration in brittle liquefiable soils", Computers and Geotechnics 134, pp. 104–123, 2021. https://doi.org/10.1016/j.compgeo.2021.104123

Oñate, E., Idelsohn, S.R., Del Pin, F., Aubry, R., "The particle finite element method – an overview", International Journal of Computational Methods 1, issue 2, pp. 267–307, 2004. https://doi.org/10.1142/S0219876204000204

Perzyna, P., "Fundamental problems in viscoplasticity", Advances in Applied Mechanics 9, pp. 243-377, 1966.

Pinedo, P., Besenzon, D., Mánica, M., Arroyo, M., Gens, A., "Exploring Viscous Effects on Numerical Simulations of Static Liquefaction Triggering", Proceedings of the 8th International Conference on Tailings Management (Tailings 2022), Online, 2022.

Robinson, S., "Rate Effect Behaviour of Different Clays from High Speed Triaxial Element Testing", Doctoral thesis, University of Dundee, 2019.

Roy, M., Tremblay, M., La Rochelle, P., "Development of pore pressures in quasi-static penetration tests in sensitive clay", Canadian Geotechnical Journal 19, issue 2, pp. 124–138, 1982. https://doi.org/10.1139/t82-015

Steiner, A., Kopf, A.J., L'Heureux, J.S., Kreiter, S., Stegmann, S., Haflidason, H., Moerz, T., "In situ dynamic piezocone penetrometer tests in natural clayey soils – a reappraisal of strain-rate corrections", Canadian Geotechnical Journal 51(4), pp. 272–288, 2014. https://doi.org/10.1139/cgj-2013-0048

Yu, H.S., "CASM: a unified state parameter model for clay and sand", International Journal for Numerical and Analytical Methods in Geomechanics 22, issue 8, pp. 621–653, 1998. https://doi.org/10.1002/(SICI)1096-9853(199808)22:8%3C621::AID-NAG937%3E3.0.CO;2-8